

# Simulation of diffraction dissociation in quark-diquark representation

V.M. Grichine<sup>a</sup>

Lebedev Physical Institute, Moscow, Russia

Received: date / Revised version: date

**Abstract.** A low mass single diffraction dissociation mode based on the quark-diquark representation of hadron-nucleon interaction is proposed. The mass spectra of nucleon-pion system are compared with experimental data and predictions of other models. The hadron-nucleus single-diffraction cross-sections are calculated in the framework of the Glauber-Gribov model for integral cross-sections. The model predictions are compared with experimental data for the different distributions of secondary particles produced in the hadron-nucleus interactions in the momentum range 31-320 GeV/c.

**PACS.** 4 1.60.Bq , 29.40.Ka

## 1 Introduction

Diffraction dissociation (DD) or inelastic diffraction scattering has more than 60 years history. It was proposed by E.L. Feinberg and I.Ya. Pomeranchuk in 1953 and became widely known due to their seminal review paper in 1956 [1]. A short time later, Good and Walker [2] proposed the general approach to DD based on the quantum field framework. These ideas were transformed to a working model by Drell and Hiida [3] and Deck [4]. The resulting Drell-Hiida-Deck (DHD) model was broadly used for the description of experiential data, see review [5]. The DHD-model was capable to describe the main features of DD, however the low mass spectra of excited hadrons are not correctly predicted by the DHD model (see Fig.3 and the references in there).

In this paper, a low mass single diffraction dissociation model based on the quark-diquark representation of hadron-nucleon interaction is proposed. The mass spectra of the nucleon-pion system are compared with experimental data and the predictions of other models. The hadron-nucleus single-diffraction cross-sections are calculated in the framework of the Glauber-Gribov model for integral cross-sections. The model predictions are compared with experimental data for the different distributions of secondary particles produced in the hadron-nucleus interactions in the momentum range 31-320 GeV/c.

## 2 Diffraction dissociation model

Fig. 1 shows the quark-diquark (qQ) diagram for the low mass (near the mass threshold  $\sim 1$  GeV for nucleons) diffrac-

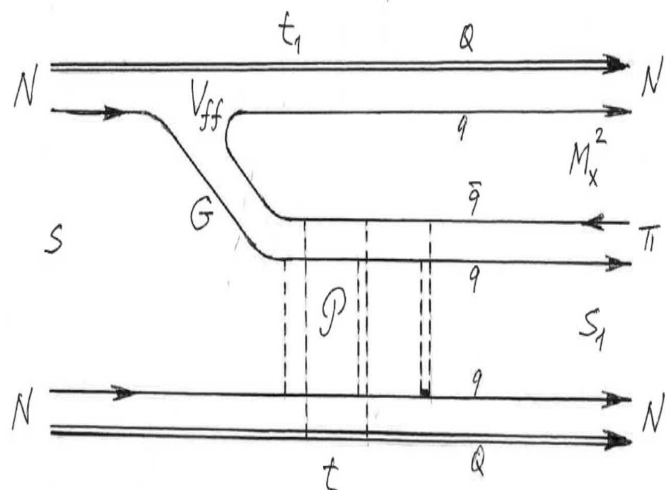


**Fig. 1.** The quark-diquark diagram for the diffraction dissociation of nucleon  $N$  in the nucleon-nucleon interaction.  $M_x^2$  is the invariant mass of the excited nucleon squared,  $t$  is the momentum transfer between nucleons.

tion dissociation of the projectile nucleon  $N$  in the nucleon-nucleon interaction.  $M_x^2$  is the invariant mass of the dissociated nucleon squared,  $t$  is the momentum transfer between nucleons,  $\sqrt{s}$  is the total energy in the center of mass system of interacting nucleons. The diffraction dissociation amplitude  $A_{dd}$  corresponding to the diagram reads:

$$A_{dd} \sim V_{ff}(t_1)G(t_1)A_{el}^{N\pi}(s_1, t),$$

where  $V_{ff}(t_1) = \exp(-\alpha't_1)$  is the vertex form-factor,  $G(t_1)$  is the  $q\bar{q}$  propagator, and  $A_{el}^{N\pi}(s_1, t)$  is the elastic amplitude according to the  $qQ$ -model with one or two

<sup>a</sup> visitor at CERN, e-mail: Vladimir.Grichine@cern.ch

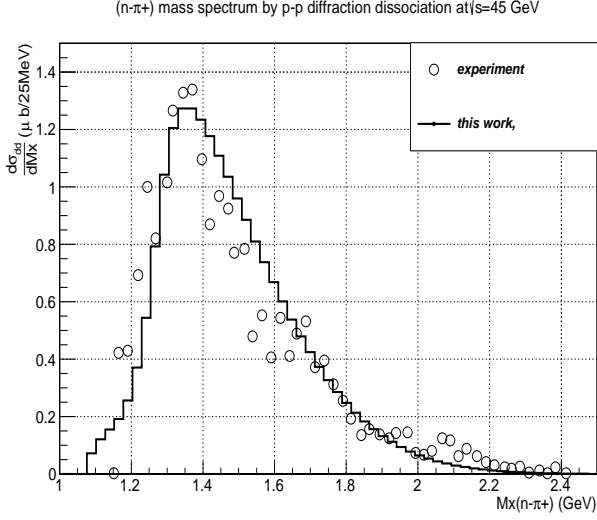


**Fig. 2.** The invariant mass spectrum of the proton-pion system produced in the proton-proton interactions at  $\sqrt{s} = 45$  GeV. The histogram corresponds to calculations according to this work, the points are experimental data [9].

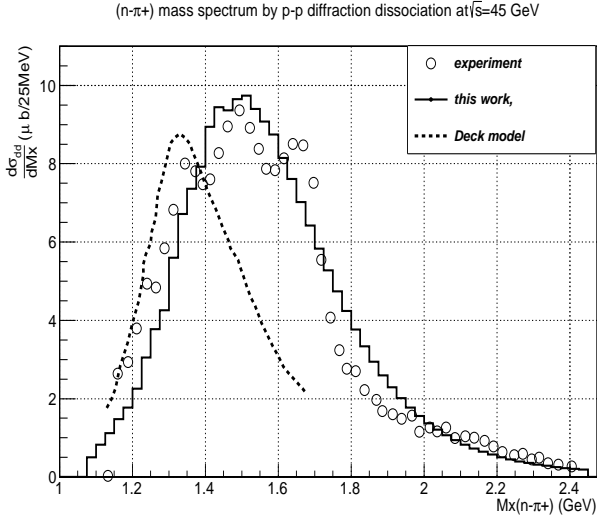


**Fig. 3.** The invariant mass spectrum of the proton-pion system produced in the proton-proton interactions at  $\sqrt{s} = 45$  GeV. The solid histogram corresponds to calculations according to this work, the dashed line is the Deck-model calculations from [8], the points are experimental data [9].

springy Pomeron  $\mathcal{P}$  exchange [6].  $t_1$  is the momentum transfer squared of the dissociated nucleon and  $s_1$  is the total momentum squared of elastic scattering. The propagator  $G(t_1)$  can be written in the Reggeized form [4,7]:

$$G(t_1) = \frac{\exp \left\{ \alpha' (t_1 - \mu^2 + i\Gamma) \ln \left[ \frac{M_x^2 - M_N^2}{\xi_o} \right] \right\}}{\alpha' (t_1 - \mu^2 + i\Gamma)},$$

where  $\mu$  is the pion mass (the efficient mass of quark-antiquark intermediate state),  $M_N$  is the mass of dissociated nucleon,  $\alpha' = 0.9 \text{ GeV}^2$ ,  $\xi_o = 1 \text{ GeV}^2$  and we in-

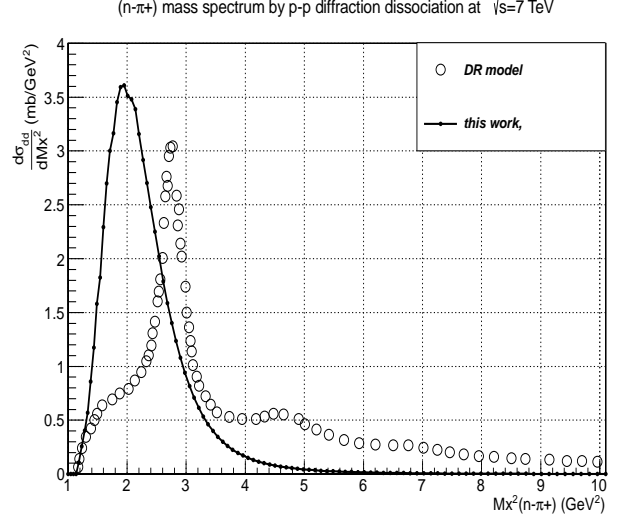


**Fig. 4.** The invariant mass spectrum of the proton-pion system produced in the proton-proton interactions at  $\sqrt{s} = 7$  TeV. The solid line corresponds to calculations according to this work, the points are calculations [10].

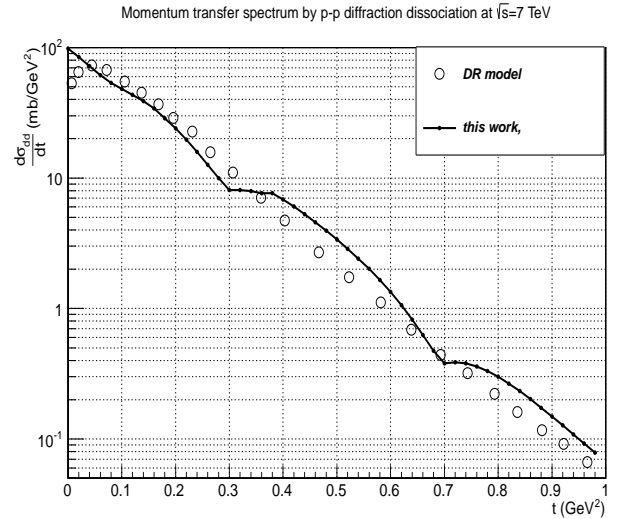


**Fig. 5.** The momentum transfer spectrum of the proton-pion system produced in the proton-proton interactions at  $\sqrt{s} = 7$  TeV. The solid line corresponds to calculations according to this work, the points are calculations [10].

roduce the imaginary part of the propagator pole,  $\Gamma = 0.09 \text{ GeV}^2$ . The latter value was chosen from the comparisons of the  $M_x$ -spectra with measurements.

The low mass single diffraction dissociation spectrum reads [8]:

$$\frac{d\sigma}{dM_x^2} = A \int dt d\cos\theta d\phi \frac{q_N}{M_x} |A_{dd}|^2,$$

where  $\theta$ ,  $\phi$  and  $q_N$  are the polar and azimuthal angles and the magnitude of the nucleon momentum in the rest system of  $N\pi$  (the Gottfried-Jackson system).  $A$  is the phase-space normalization constant. The single diffraction

dissociation model was compared with experimental data in terms of  $d\sigma/dM_x$ ,

$$\frac{d\sigma}{dM_x} = 2M_x \frac{d\sigma}{dM_x^2},$$

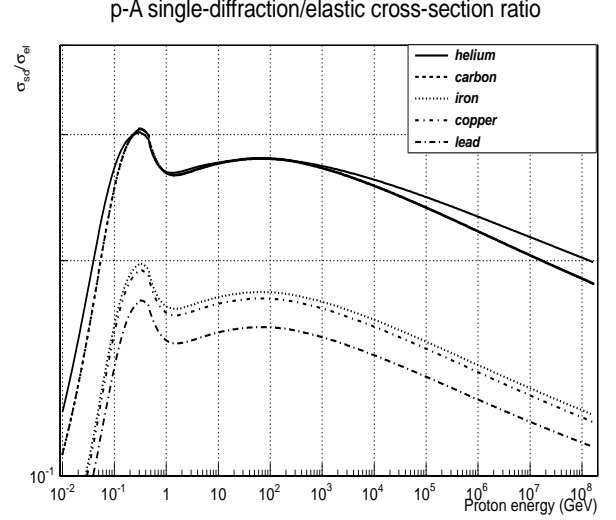
the invariant differential cross-sections. The data were taken from [9] for  $p+p \rightarrow (n\pi^+) + p$  reaction at CERN ISR  $\sqrt{s}=45$  GeV. The detector acceptance covers  $0 < \phi < 2\pi$  and different ranges of  $\cos\theta$  and  $|t|$  depending on the analysis of events.

Fig. 2 shows the invariant mass spectrum of the proton-pion system produced in the proton-proton interactions at  $\sqrt{s} = 45$  GeV. The histogram corresponds to calculations according to this work, the points are experimental data [9]. Both the data and simulation correspond to  $-0.3 < \cos\theta < 0.3$  and  $0.05 < |t| < 0.2$  GeV<sup>2</sup>. Fig 3 shows the invariant mass spectrum of the proton-pion system produced in the proton-proton interactions at  $\sqrt{s} = 45$  GeV. The solid histogram corresponds to calculations according to this work, the dashed line is the Deck-model calculations from [8], the points are experimental data [9]. Both the data and simulation correspond to  $-0.3 < \cos\theta < 1$  and  $0.05 < |t| < 1.2$  GeV<sup>2</sup>. One can see that the proposed model shows good agreement with data for the invariant mass spectrum.

The model predictions for the proton-proton diffraction dissociation at the LHC energies are shown in Figs. 4-5. Fig. 4 shows the invariant mass spectrum of the proton-pion system produced in the proton-proton interactions at  $\sqrt{s} = 7$  TeV. The solid line corresponds to calculations according to this work, the points are calculations according to the dual Reggeon (DR) model [10]. Both calculations correspond to  $-1 < \cos\theta < 1$  and  $0 < |t| < 1$  GeV<sup>2</sup>. Fig. 5 shows the momentum transfer spectrum of the proton-pion system produced in the proton-proton interactions at  $\sqrt{s} = 7$  TeV. The solid line corresponds to calculations according to this work, the points are calculations [10]. Both calculations correspond to  $-1 < \cos\theta < 1$  and  $0 < |t| < 6$  GeV<sup>2</sup>. It is seen that the mass spectra differ, while the momentum transfer spectra are more consistent. Experimental data are needed to resolve the observed disagreement.

### 3 Simulation framework

The GEANT4 simulation tool-kit [11] was chosen as the framework for the simulation of the low mass diffraction dissociation according to the proposed model. The simulation implementation consists of the single diffraction hadron-nucleus cross-section model, the model final state generator and the GEANT4 application allowing one to reproduce approximately the experimental set-ups.



**Fig. 6.** The ratio of the single diffraction to elastic cross-section for the proton-nucleus interactions versus the proton energy.

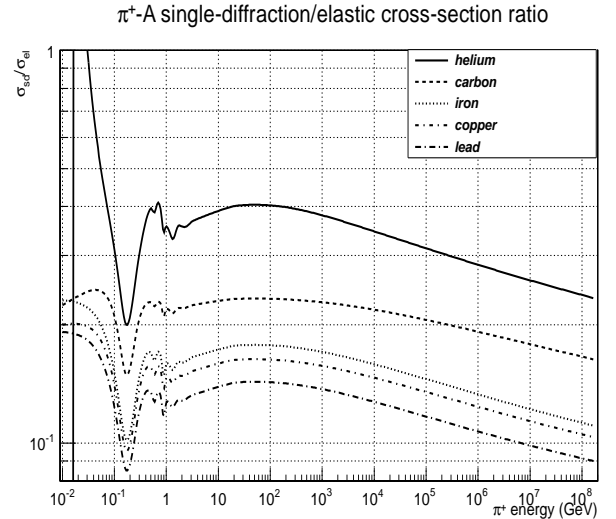


**Fig. 7.** The ratio of the single diffraction to elastic cross-section for the pion-nucleus interactions versus the pion energy.

#### 3.1 Single diffraction cross-section

In the framework of simplified Glauber-Gribov model [12] the cross sections read:

$$\sigma_{tot}^{hA} = 2\pi R^2 \ln \left[ 1 + \frac{A\sigma_{tot}^{hN}}{2\pi R^2} \right], \quad \sigma_{in}^{hA} = \pi R^2 \ln \left[ 1 + \frac{A\sigma_{tot}^{hN}}{\pi R^2} \right],$$

$$\sigma_{prod}^{hA} = \pi R^2 \ln \left[ 1 + \frac{A\sigma_{in}^{hN}}{\pi R^2} \right], \quad \sigma_{qe}^{hA} = \sigma_{in}^{hA} - \sigma_{prod}^{hA},$$

$$\sigma_{sd}^{hA}(hA \rightarrow XA) = \pi R^2 \{ \alpha - \ln[1 + \alpha] \},$$

$$\alpha = \frac{A\sigma_{tot}^{hN}}{2\pi R^2 + A\sigma_{tot}^{hN}}.$$

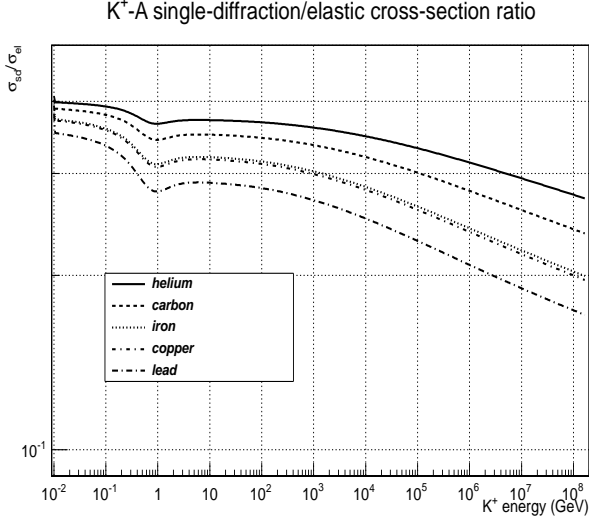


**Fig. 8.** The ratio of the single diffraction to elastic cross-section for the kaon-nucleus interactions versus the kaon energy.

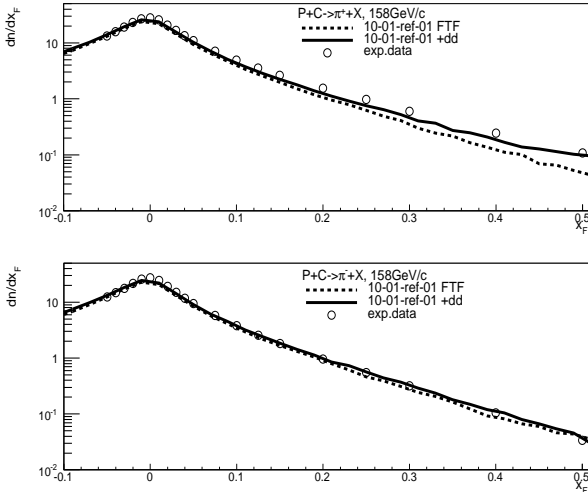


**Fig. 9.** The  $x_F$ -distribution of secondary  $\pi^+$  (upper) and  $\pi^-$  (lower) produced in the proton-carbon interactions with the proton momentum 158 GeV/c. The solid line - the FTF model with low mass DD, the dashed line - the FTF model, the points are the NA49 data [13].

Where  $\sigma_{tot}^{hA}$ ,  $\sigma_{in}^{hA}$ ,  $\sigma_{prod}^{hA}$ ,  $\sigma_{qe}^{hA}$  and  $\sigma_{sd}^{hA}$  ( $hA \rightarrow XA$ ) are the total, inelastic, production, quasi-elastic and single-diffraction (responsible for low mass DD) cross sections of a hadron on a nucleus  $A$ , respectively. The total and inelastic hadron-nucleon cross-sections are  $\sigma_{tot}^{hN}$  and  $\sigma_{in}^{hN}$ , respectively.  $R$  is the nucleus radius. In this framework the cross-sections are subdivided as follow:

$$\sigma_{el}^{hA} = \sigma_{tot}^{hA} - \sigma_{in}^{hA} = \sigma_{coh-el}^{hA} + \sigma_{sd}^{hA}(hA \rightarrow XA),$$

where  $\sigma_{coh-el}^{hA}$  is the coherent elastic cross-section. The Glauber-Gribov cross-sections are the part of the GEANT4

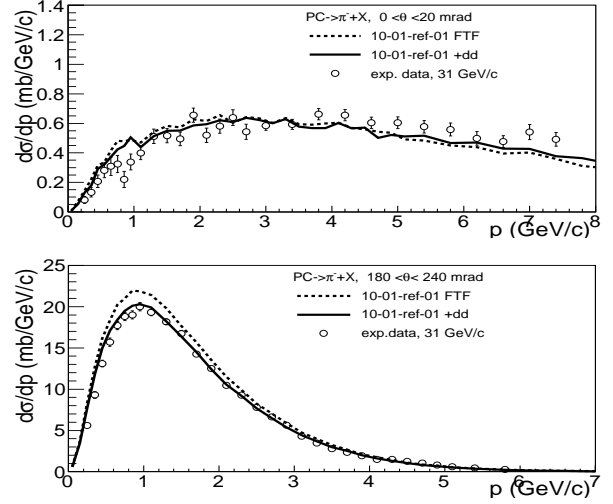


**Fig. 10.** The momentum distribution of secondary  $\pi^-$  produced in the proton-carbon interactions with the proton momentum 31 GeV/c. The upper plot corresponds to the scattering angles 0-20 mrad, the lower - 180-240 mrad. The solid line - the FTF model with the low mass DD, the dashed line - the FTF model, the points are the NA61 data [14].

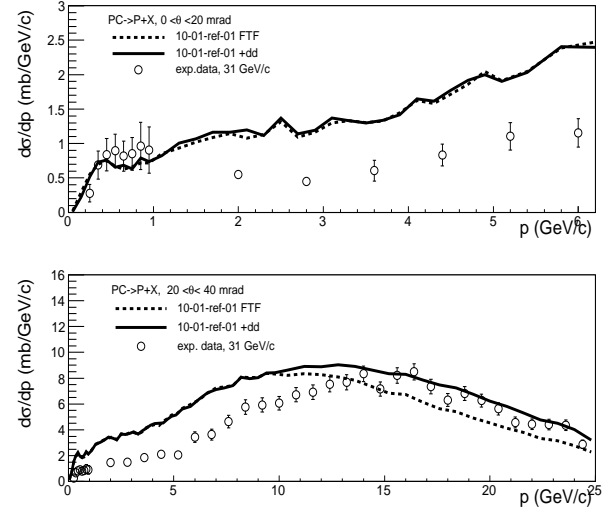


**Fig. 11.** The momentum distribution of secondary protons produced in the proton-carbon interactions with the proton momentum 31 GeV/c. The upper plot corresponds to the scattering angles in the range 0-20 mrad, the lower - 20-40 mrad. The solid line - the FTF model with the low mass DD, the dashed line - the FTF model, the points are the NA61 data [14].

library, therefore one can introduce the low mass DD generator via the ratio  $\sigma_{sd}^{hA}(hA \rightarrow XA)/\sigma_{el}^{hA}$ .

### 3.2 Final state generator

The corresponding generator was implemented in the framework of the GEANT4 tool-kit. This library allows one to implement the hadron elastic process modified so that it

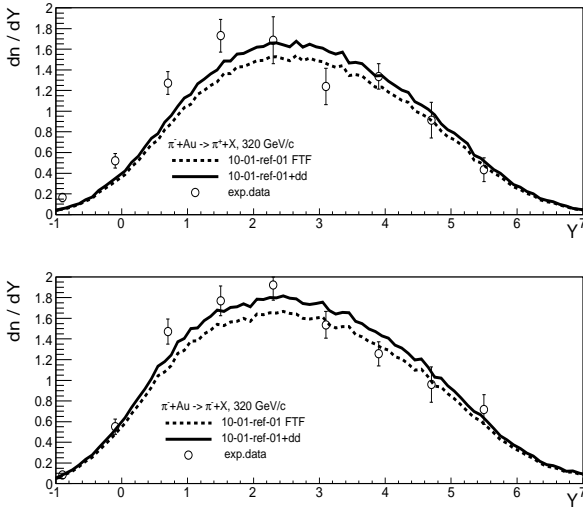


**Fig. 12.** The rapidity distribution of secondary  $\pi^+$  (upper) and  $\pi^-$  (lower) produced in the  $\pi^-$ -gold interactions with the  $\pi^-$  momentum 320 GeV/c. The solid line - the FTF model with the low mass DD, the dashed line - the FTF model, the points are the E597 data [15].

activates the low mass DD generator with the probability equal to the  $\sigma_{sd}/\sigma_{el}$  ratio. The generator utilizes the pre-calculated model mass spectrum to excite and retard the projectile hadron. The sampled  $M_x$  value affects the longitudinal momentum transfer between the projectile and the target nucleon. The excited hadron experiences elastic scattering on the target nucleon according to the pre-calculated transverse momentum spectrum. A proper excited hadron resonance (f.e. for nucleons, these are  $N(1440)$ ,  $N(1520)$  and  $N(1680)$ ) is selected according to the mass spectrum and the reaction kinematics. Then the resonance is decayed recursively down to not short-lived particles. The latter produce the final state of the low mass DD generator and are subject of the further GEANT4 tracking.

### 3.3 Simulation application

A GEANT4 application was implemented creating simplified geometries of few experiments. The geometry includes the volume target with both material and sizes modified from the command line. The target was surrounded by the sensitive detector volume where the secondary tracks were analyzed in terms of their kinematics. The application physics list allows a user to change the active physics, in particular to switch on/off the DD generator.

## 4 Comparison with experimental data

The spectra of secondary particles produced in the inelastic hadron-nucleus interactions measured in different thin target experiments we used for the low mass DD generator validation. The GEANT4 FTFP\_BERT physics list was

used in two modes - with and without the low mass DD generator activation.

Fig. 9 shows the  $x_F$ -distribution of secondary  $\pi^+$  (upper) and  $\pi^-$  (lower) produced in the proton-carbon interactions with the proton momentum 158 GeV/c. The solid line - the FTF model with the low mass DD, the dashed line - the FTF model, the points are the NA49 data [13]. The longitudinal scaling variable  $x_F$  is defined in the center of mass system of the projectile proton and the target nucleon:

$$x_F = \frac{2p_L}{\sqrt{s}},$$

where  $p_L$  is the longitudinal secondary particle momentum and  $\sqrt{s}$  is the total energy of the projectile proton and the target nucleon. It is seen that the low mass DD generator increases the spectrum in the region of high  $x_F$ , which corresponds to forward kinematics region of secondary pion. This correction improves the agreement between the measurement and the simulation.

Fig. 10 shows the momentum distributions of secondary  $\pi^-$  produced in the proton-carbon interactions with the proton momentum 31 GeV/c. The upper plot corresponds to the scattering angles 0-20 mrad, the lower - 180-240 mrad. The solid line - the FTF model with low mass DD, the dashed line - the FTF model, the points are NA61 data [14]. One can see that the low mass DD correction improves the agreement with the experiment especially in the scattering angle range 180-240 mrad. Fig. 11 shows the momentum distributions of secondary protons produced in the proton-carbon interactions with the proton momentum 31 GeV/c. The upper plot corresponds to the scattering angles in the range 0-20 mrad, the lower - 20-40 mrad. The solid line - the FTF model with the low mass DD, the dashed line - the FTF model, the points are the NA61 data [14]. The low mass DD correction improves essentially the agreement with the data in the angle range 20-40 mrad.

Fig 12 shows the rapidity distributions of secondary  $\pi^+$  (upper) and  $\pi^-$  (lower) produced in the  $\pi^-$ -gold interactions with the  $\pi^-$  momentum 320 GeV/c. The solid line - the FTF model with the low mass DD, the dashed line - the FTF model, the points are the E597 experiment data [15]. The rapidity of secondary pions corresponds to the laboratory frame. The low mass DD activation results in better agreement with the data.

## 5 Summary

The low mass single diffraction dissociation model based on the quark-diquark representation of hadron-nucleon interaction is proposed. The mass spectra of the nucleon-pion system are compared with experimental data and the predictions of other models. It was found better agreement with the data compared to the DHD model. The reason is that the proposed model utilizes the modified propagator  $G(t_1)$  with increased imaginary part due to introduction of the  $\Gamma$ -parameter. The hadron-nucleus single-diffraction cross-sections are calculated in the framework

of the Glauber-Gribov model for integral cross-sections. The model predictions are compared with the experimental data for the different distributions of secondary particles produced in hadron-nucleus interactions in the momentum range 31-320 GeV/c. The comparisons show that the DD generator improves the agreement with the experimental data. The model and the generator tuning as well as extended comparisons with experimental data are in progress and will be reported elsewhere.

## Acknowledgment

The author is thankful to S. Bertolucci, S. Giani and M. Mangano for stimulating discussions and support. V. Ivanchenko and A. Ribon presented the interface for the model introducing in the framework of GEANT4 .

## References

1. I. Ya. Pomeranchuk and E.L. Feinberg, *Dokl. Akad. Nauk SSSR* **93** (1953) 439; E.L. Feinberg and I. Pomeranchuk, *Del Nuov. Cim. Suppl.* **v. III, s. X** (1956) 652.
2. M.L. Good and W.D. Walker, *Phys. Rev.*, **120** (1960) 1857.
3. S.D. Drell and K. Hiida, *Phys. Rev. Lett.*, **7** (1961) 199.
4. R. Deck *Phys. Rev. Lett.*, **13** (1964) 169.
5. N.P. Zotov and V.A. Tsarev *Sov. Phys. Uspekhi*, **31** (1988) 119.
6. V.M. Grichine, *Eur. Phys. J.*, **Plus 129** (2014) 112.
7. V.A. Tsarev, *Phys. Rev.*, **11** (1975) 1864.
8. H.R. Gerhold and W. Majerotto, *Il Nuov. Cim.*, **A36** (1976) 271.
9. H. De Kerret, E. Nagy, M. Regler et al., *Phys. Lett.*, **B63** (1976) 483.
10. L. Jenkovszky, A. Sali, J. Turoci and D. Himics, *Odessa Astr. Pub.*, **25** (2012) 102.
11. GEANT4 Collaboration, *Nucl. Instr. and Meth.*, **A506** (2003) 250.
12. V.M. Grichine, *Eur. Phys. J.*, **C62** (2009) 399; *Nucl. Instr. and Meth.*, **B267** (2009) 2460.
13. NA49 Collaboration, *Eur. Phys. J.*, **C49** (2007) 897.
14. M.Z. Posiadata, *J. of Phys Conf. Ser.*, **408** (2013) 012048.
15. E597 Collaboration, *Z. Phys.*, **C62** (1994) 199.